Contents lists available at ScienceDirect

# Surface & Coatings Technology

journal homepage: www.elsevier.com/locate/surfcoat





# From pulsed-DCMS and HiPIMS to microwave plasma-assisted sputtering: Their influence on the properties of diamond-like carbon films

Caroline Hain a,c,d,\*, David Brown b, Alexander Welsh b, Krzysztof Wieczerzak c, Robert Weiss b, Johann Michler<sup>c</sup>, Aïcha Hessler-Wyser<sup>d</sup>, Thomas Nelis<sup>a,c</sup>

- a Bern University of Applied Sciences, Institute for Applied Laser, Photonics and Surface Technologies ALPS, Quellgasse 21, 2502 Biel/Bienne, Switzerland
- <sup>b</sup> Malachite Technologies, 2262 Palou Ave., San Francisco, CA 94124, USA
- c Empa, Swiss Federal Laboratories for Materials Science and Technology, Laboratory for Mechanics of Materials and Nanostructures, Feuerwerkerstrasse 39, 3602 Thun,
- <sup>d</sup> EPFL, École Polytechnique Fédérale de Lausanne, Laboratory for Photovoltaics and Thin Film Electronics, Rue de la Maladière 71b, 2000 Neuchâtel, Switzerland

#### ARTICLE INFO

#### Keywords: Diamond-like carbon Magnetron sputtering Microwave plasma Raman spectroscopy Nanoindentation Langmuir probe

#### ABSTRACT

The fabrication of high-hardness non-hydrogenated diamond-like carbon (DLC) via standard magnetron sputtering (MS) is often hindered by the low sputtering yields and ionisation rates of carbon, therefore investigations into pulsed alternatives of MS, else sputtered species post-ionisation methods, are of particular interest. This work focuses on investigating the influence of pulsed-direct current MS (pDCMS), high power impulse magnetron sputtering (HiPIMS) and their microwave plasma-assisted (MA-pDCMS, MA-HiPIMS) variants on the properties of the fabricated DLC films. Two setups were used for the pDCMS- and HiPIMS-based methods, respectively. The films were characterised using Raman spectroscopy, nanoindentation, X-ray reflectometry and scanning electron microscopy, where the pDCMS-produced films were additionally characterised by film-stress measurements. Moreover, in situ time-resolved Langmuir probe plasma analysis was performed under HiPIMS and MA-HiPIMS conditions to analyse the influence of the magnetron and microwave plasmas on one another. For both DCMSand HiPIMS-based procedures, it was found that the addition of microwave plasma did not facilitate attaining hardnesses beyond 30 GPa, however, it did enable modifying the morphology of the films. Furthermore, this study shows the potential of synchronised sputtering with substrate biasing, as well as the importance of microwave plasma source positioning in relation to the substrate.

## 1. Introduction

Diamond-like carbon (DLC) is an amorphous carbon material, where its chemical and mechanical properties have made it an attractive choice for films in applications related to automotive and aerospace industries, biomedicine, magnetic storage media and many others [1-6]. The mechanical and optical properties of DLC primarily stem from sp<sup>3</sup> and sp<sup>2</sup> carbon atom hybridisations, where diamond, composed of 100 % sp3, is extremely hard (approx. 100 GPa) and transparent, whereas graphite, composed of 100 % sp<sup>2</sup>, is rather soft (<5 GPa) and opaque [4]. Therefore, acquiring the ability to control sp<sup>2</sup> and sp<sup>3</sup> formation within the fabricated DLC films would allow to tune the material's properties for specific applications.

There exist different techniques for the fabrication of DLC thin films,

with chemical (CVD) and physical vapour deposition (PVD) and their variations [7,8] being among the most popular. CVD uses gaseous hydrocarbon precursors as the source of carbon, therefore hydrogenated DLC films are obtained. During PVD, the carbon source is can be a pure carbon target, enabling the production of non-hydrogenated amorphous carbon (a-C) and tetrahedral amorphous carbon (ta-C) films. Such films exhibit higher hardness, greater temperature [9-11] stability and under humid conditions [12-14] than their hydrogenated counterparts. The mechanism behind sp<sup>2</sup> and sp<sup>3</sup> formation, i.e. subplantation, occurring during PVD-based fabrication is schematically shown in Fig. 1. Subplantation occurs through direct carbon ion penetration into the film's surface and/or indirectly through the displacement of surface atoms into interstitial sites. This entails the penetration of impinging hyperthermal species, ranging from 1 to 1000 eV, into the top layers of the growing

E-mail address: caroline.hain@bfh.ch (C. Hain).

<sup>\*</sup> Corresponding author at: Bern University of Applied Sciences, Institute for Applied Laser, Photonics and Surface Technologies ALPS, Quellgasse 21, 2502 Biel/ Bienne, Switzerland.

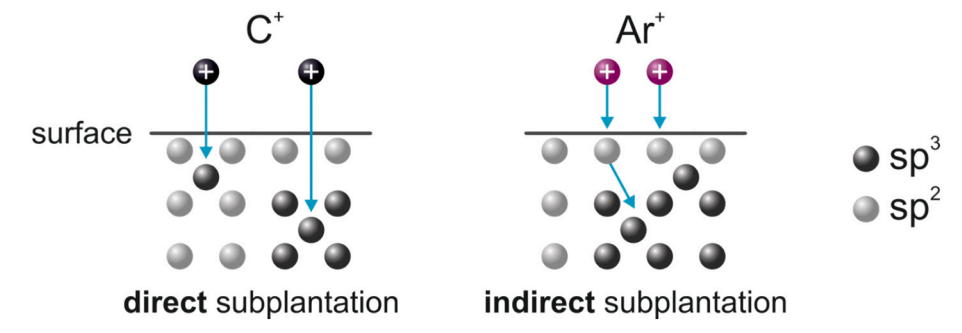


Fig. 1. Deposition (sp $^2$  and sp $^3$  formation) mechanisms of DLC through direct (carbon ion film penetration) and indirect (displacement of surface carbon atoms through argon ion bombardment) subplantation, adapted from [4,16].

film, inducing sp<sup>2</sup> to sp<sup>3</sup> transformations. As graphitic structures exhibit a lower displacement energy than diamond ones (25 eV vs 80 eV), they will be preferentially displaced upon ion bombardment [15].

Carbon is characterised by a low ionisation rate [17], and high ionisation potential [18], therefore high plasma densities are beneficial for creating carbon ions. With increased plasma densities, more argon atoms can be ionised, additionally leading to more electrons being present in the plasma. The presence of both can facilitate carbon ionisation either through argon ion-carbon collisions and energy transfer or electron-carbon collisions. Direct-current magnetron sputtering (DCMS) is characterised by low plasma densities (10<sup>14</sup>÷10<sup>16</sup> m<sup>-3</sup>) and low degrees of ionisation [19]. At the other end of the PVD spectrum is cathodic arc deposition (Arc-PVD), where an arc is generated to vaporise the cathode target. Here, it is possible to reach high plasma densities,  $(10^{18} \div 10^{26} \text{ m}^{-3})$  [20], however, this method often results in the formation of droplets or macroparticles of various quantities on the film's surface [21,22]. Therefore, a compromise needs to be found between these two extremes. One way of overcoming these issues is moving towards pulsed-DCMS (pDCMS) [23,24], and its further extension high power impulse magnetron sputtering (HiPIMS) technique. In this case, high power densities are applied in short pulses, facilitating the generation of highly ionised species of the sputtered material, through the generation of high plasma densities at the target (10<sup>18</sup>÷10<sup>19</sup> m<sup>-3</sup>) [20,25], and producing high-density films [18,26–28]. For DLC, it has been proven that HiPIMS enhances the deposition rate [29] and through sputtering in short, but highly energetic pulses, it facilitates the production of hard and dense DLC films [25,30-36]. An alternative method for increasing the ionisation of carbon species is the introduction of additional plasma sources. Some work has been performed in this direction for DLC films, where cylindrical microwave (MW) plasma, using the electron cyclotron effect (ECR), was combined with a DC sputter source, equipped with a cylindrical target in the down-stream configuration, however, without the presence of additional magnetic fields [37,38]. Recent developments in solid-state-based microwave generator sources [39] and associated impedance-matched applicators have allowed for the design of new reactor configurations using microwave plasma to further facilitate hybrid plasma processes.

Despite many options for producing DLC films, linking the influence of deposition parameters on the properties of DLC films or, indeed, characterising DLC properties, is not trivial. The main issues hindering DLC analysis are: (1) the problem of consistent characterisation of the influence of multiple process parameters on the produced films and their reproducibility from system to system, and (2) only a few analytical techniques provide direct answers concerning carbon structuring (sp<sup>2</sup> and sp<sup>3</sup> contents), meaning that result interpretation is required. Therefore, it is important to look not only at the properties of the film but also the deposition setup, and in turn, the deposition environment.

In this work, DLC films were deposited using two systems, via pDCMS and microwave plasma-assisted pDCMS (MA-pDCMS), as well as HiPIMS and MA-HiPIMS, respectively. The progression through these techniques, especially in the direction of including microwave plasma, and linking their characteristics to the properties of the fabricated DLC films show the different ways of producing DLC films with comparable properties, while highlighting the limitation of sputtering techniques for attaining high-hardness films.

## 2. Experimental section

## 2.1. Deposition setups

System 1, a customised high-vacuum "sputter-down" setup (Malachite Technologies, USA) used to produce DLC films via pDCMS and MA-pDCMS, is shown in Fig. 2A. The reactor is arranged in a configuration, where a  $\varnothing$  50 mm sputtering cathode (Angstrom Sciences, USA) and four

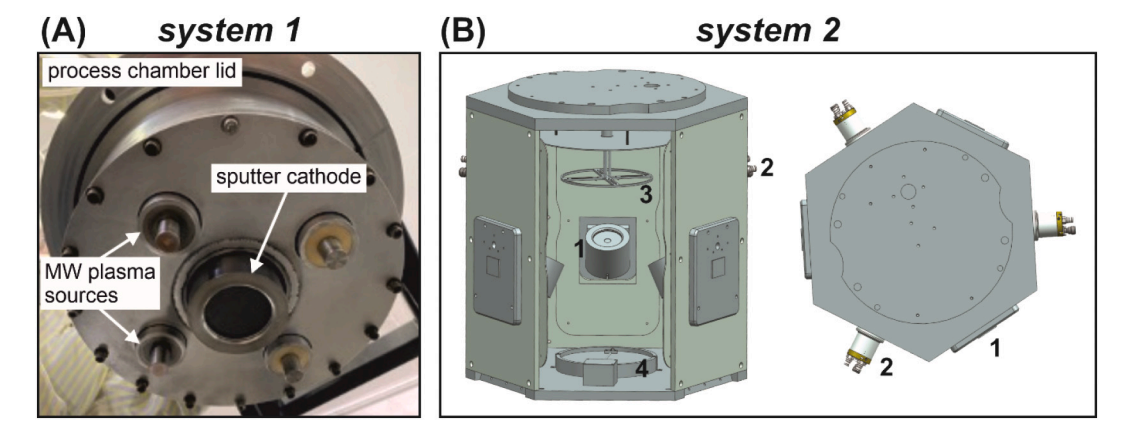


Fig. 2. Configuration of (A) system 1 for pDCMS-based processes, (B) system 2 for HiPIMS-based processes, left: front view, right: top view, 1 – magnetrons, 2 – microwave plasma sources, 3 – rotary substrate holder, 4 – butterfly valve.

Aura-Wave ECR [39] coaxial plasma sources (SAIREM, France) are installed in the reactor's lid. The microwave plasma sources are evenly spaced around the sputter cathode, 75 mm from centre and positioned nearly planar with the sputtering target's surface. The sputter cathode power supply (Advanced Energy, USA) is configured to operate in unipolar negative pulsed-DC power control mode. Each Aura-Wave plasma source is connected by a LMR400 type coaxial cable to discrete variable power output 200 W, 2.45 GHz solid state microwave generators (SAIREM, France). The solid-state generators have built-in frequency tuning functions to allow for minimizing reflected power and efficient coupling of the microwave power into the plasma load. The system is evacuated via a TPH 2301 turbomolecular pump (Pfeiffer Vacuum, Germany), backed up by an XDS35i dry scroll pump (Edwards Vacuum, UK), to reach a minimum base pressure of approx.  $6 \times 10^{-5}$  Pa. The plasma gas supply is controlled via a 200 sccm mass-flow controller (MKS Instruments, USA), and enters the chamber through a connection in the chamber's wall. Substrates are introduced into the process chamber by means of a load-lock sample transfer chamber and are placed on a Ø 150 mm substrate stage and positioned 75 mm below the sputtering target. The substrate stage is electrically isolated and connected to a MDX series DC power supply (Advanced Energy, USA) configured to operate at constant voltage and provides the means to bias the substrate to a negative potential during film deposition.

System 2 (Fig. 2B) is a HEXL Modular Deposition System, equipped with 3 magnetrons in unbalanced configuration (Korvus Technology, UK). The chamber is evacuated via a TC 400 turbomolecular pump (Pfeiffer Vacuum, Germany), backed up by an SH-110 dry scroll vacuum pump (Agilent Technologies, USA). The interspace of the double O-ring system is evacuated by an IDP-3 dry scroll vacuum pump (Agilent Technologies, USA). In this configuration, the maximum flow rate allowing for stable operation is 120 sccm of argon, where the flow rate is controlled via a 200 sccm mass-flow controller (Teledyne Hastings Instruments, USA). The gas enters the chamber through the three installed magnetrons. The system allows for reaching a minimum base pressure of approx.  $2 \times 10^{-5}$  Pa. A full range compact gauge (Pfeiffer Vacuum, Germany) is used to determine the pressure inside the reactor. Further

 Table 1

 Cleaning and pre-treatment process summary.

system	ex situ cleaning	in situ cleaning				
		MW power (W)	Ar flow (sccm)	bias (V)	pressure (Pa)	time (min)
1	compressed air blowing	3×100	100	-100	0.5	1
2	5 min ultrasonic cleaning in acetone and isopropanol	3×50	10	-600	0.2	10

**Table 2**Selected process parameters for DLC film deposition.

substrate bias (V) pressure (Pa) Ar flow (sccm) microwave power (W) system process type 0 pulsed direct-current magnetron sputtering (pDCMS) -100 1 0.5 100 3×45 microwave plasma-assisted pDCMS (MA-pDCMS)  $3 \times 100$ -100 3×200 110 0.6 60 high power impulse magnetron sputtering (HiPIMS)  $0 \div -350$ 2 0.4 60  $0 \div -300$ microwave plasma-assisted HiPIMS (MA-HiPIMS) 0.4 60 3×50 - 250 pulsed

details can be found in the Supplementary Information (SI). For inducing pulsed sputtering, HiPIMS HiPSTER 1-type generators (Ionautics, Sweden) were used, whereas the previously-described Aura-Waves and solid-state microwave generators (SAIREM, France) were used for creating the microwave volume plasma. The magnetrons and microwave generators were placed alternately on each chamber wall. A rotary sample holder was attached to the lid of the chamber and the distance between the magnetrons and the substrates was approx. 120 mm. A GEN 1U 750 W power supply (TDK-Lambda, Japan) was connected to the rotary substrate holder using a coaxial cable via a sliding contact installed between the inner and outer part of the holder's rotation axis. The grounding was attached to the chamber's body. This enabled supplying a bias voltage, variable between 0 and - 600 V, to the substrate to manipulate ion behaviour in its vicinity. The bias voltage stability at the substrate holder during HiPIMS operation was measured to be better than 1 %.

## 2.2. DLC film fabrication

Series of DLC films were fabricated using the previously described equipment, by means of DC-bias pDCMS, MA-pDCMS, HiPIMS, MA-HiPIMS and pulsed-bias MA-HiPIMS. Both systems used Ø 50 mm 99.999 % purity graphite disc (Kurt J. Lesker Company, USA) as the sputtering targets, 6 mm and 3 mm thick for system 1 and 2, respectively. In both cases, the substrates were  $\emptyset$  50 mm  $\langle 100 \rangle$ -oriented silicon wafers (system 1 University Wafer, Inc., USA, system 2 MicroChemicals, Germany). Once the substrates were cleaned ex situ, they were placed inside the deposition chamber, where they were subjected to a pre-treatment procedure. The aim of this process is to remove organic pollutants and native oxides from the substrates' surfaces by being exposed to microwave plasma, inducing so-called sputter cleaning. Ultra-high purity argon was used as the plasma-forming gas (system 1: County Specialty Gases, USA, system 2: Carbagas, Switzerland). This step additionally aims at improving the adhesion between the substrate and deposited film. A summary of substrate cleaning and pre-treating is presented in Table 1.

The deposition process is initiated directly after the pre-treatment process without breaking vacuum. The magnetrons are switched on while the microwave-generated plasma is on to avoid the redeposition of contaminants and/or reoxidation. For non-MW processes, the microwave generators were turned off once the plasma surrounding the magnetrons was stable. Otherwise, the microwave generators remained on for the duration of the process. A total of five DLC film series were deposited. System 1 was used for pDCMS and MA-pDCMS, where for all depositions the pulse-off settings were fixed at 0.4  $\mu s$  with a repetition rate of 100 kHz and constant sputtering power of 300 W. System 2 was used to for HiPIMS and MA-HiPIMS, where the HiPSTER units were operated in a peak current limiting mode, i.e. the voltage regulation was set to assure a constant peak current of 30 A. The HiPIMS pulse length

a direct-current substrate bias, unless noted otherwise

<sup>&</sup>lt;sup>b</sup> pulsing frequency 600 Hz

was set to  $30 \,\mu s$  with a repetition rate of 600 Hz. A summary of the used deposition parameters is presented in Table 2.

## 2.3. Deposition environment analysis

Detailed deposition environment analyses were conducted for HiPIMS-based processes. The voltage and current outputs signals supplied by the HiPSTER units were monitored using a mixed signal oscilloscope (Tektronix, USA). Data were acquired using the averaging mode, based on 128 pulses.

Plasma properties in the vicinity of the substrate were obtained by means of Langmuir single probe (Impedans, Ireland) measurements under microwave plasma, HiPIMS and combined MA-HiPIMS conditions. The chamber properties selected for these tests were 0.4 Pa with 60 sccm of Ar. The Langmuir probe consisted of a  $\oslash$  0.4 mm, 10 mm tip and a DC reference. A voltage sweep from – 20 to 30 V, with a step of 0.5 V, was performed and the resulting current was tracked. The probe was positioned at the height where the substrate would be. Microwave plasma characterisation was completed in time-averaged mode, whereas HiPIMS and MA-HiPIMS conditions were investigated in time-resolved mode using a HiPSTER Sync Unit (Ionautics, Sweden) as the external trigger. The HiPIMS pulse was set to start after 20  $\mu$ s of delay in respect to the Langmuir probe measurement in all cases.

Temperature measurements, using a  $\oslash 1$  mm, 50 mm custom-made microwave plasma-resistant temperature probe (Mesurex, France), were performed at substrate height to evaluate sample heating during sputtering and under microwave plasma conditions.

## 2.4. Film analysis

Raman spectroscopy via an inVia dispersive Raman System H45383 equipped with a green 514 nm laser (Renishaw, UK) was used to determine the type of bonds present in the DLC films and evaluate the  $\rm sp^2$  and  $\rm sp^3$  hybridization contents. The gathered spectra were processed through background removal and double Gaussian D and G peak fitting to extract G peak position, D to G peak intensity ratios ( $\rm I_D/I_G$ ), and G peak full width at half maximum (FWHM).

DLC film densities were obtained via X-ray reflectivity (XRR) using a D8 Discover X-Ray Diffractometer (Bruker, USA). The incident beam (Cu  $K\alpha$ ) was conditioned using a Göbel mirror. The measurements were done in  $\theta{-}2\theta$  geometry and the reflectivity patterns were analysed by fitting the data to a physical model, created by selecting a silicon base with a SiO $_2$  layer and a carbon layer on top, using the DIFFRAC LEPTOS 7 software (Bruker, USA). Measurement uncertainty was determined to be in the range of 5 %.

The thickness and stress of the films produced via *system 1* were measured using a Dektak IIA stylus profilometer (Bruker, USA). Film stress measurements were performed to correlate the obtained results against film hardness and provide initial process feedback. The profilometer was set to a scan length of 40 mm, after which the Dektak IIA software calculated the radius of curvature of the wafer surface and compared it against a similar scan taken on the wafer prior to depositing. From the resulting change in curvature, the software used the Stoney equation [40] to calculate the film stress based on known material properties and film thickness.

Samples produced by both systems were cleaved and their fracture cross-sections, as well as their surface morphology, were imaged using a Hitachi S-4800 high-resolution cold field emission (CFE) scanning electron microscope (SEM) (Hitachi High-Tech Corporation, Japan).

The hardness and elastic modulus of all DLC films were determined by means of nanoindentation using a Hysitron Ubi Nanoindenter (Bruker, USA). Different indenter tips were used, depending on film series thickness, to prevent exceeding penetration depths greater than 10 % of the films' thickness [41], while obtaining plastic deformation for reliable hardness measurements. Films deposited via *system 1* were measured using a diamond cube corner tip (for shallow indents and low

loads), whereas films fabricated via *system 2* using a diamond Berkovich indenter tip. Machine compliance was adjusted accordingly for a given tip. The tip area function was calibrated on fused silica for each tip separately in the relevant measurement range. For obtaining a representative average, 16 indents were performed on each film. The maximum load value was held constant for 2 s, whereas loading and unloading each lasted 5 s. Load-displacement curves were analysed by applying the Oliver and Pharr approach [42], using 0.2 for the Poisson's ratio of DLC [43,44].

#### 3. Results

The pDCMS- and HiPIMS-based processes, although closely resembling one another, are different in terms of their sputtering characteristics. The comparison of these techniques aims to provide an improved understanding on the correlation between the generated deposition environment, especially plasma conditions, and the properties of the fabricated DLC films.

#### 3.1. pDCMS-based DLC films

XRR was performed on the pDCMS and MA-pDCMS films to determine their thickness and density. To facilitate the fitting procedure, the thicknesses of the films were evaluated first using a profilometer. The results from profilometer measurements and those obtained from the XRR fitting procedure are similar, as can be seen in Table 3. Film densities differ depending on the fabrication method. The grounded pDCMS sample has the lowest density, which is increased by applying a negative bias of –100 V. Further film densification was obtained by applying the additional microwave plasma in the vicinity of the sputter target. The obtained densities are on the higher end of those reported previously [25,45].

Afterwards, the samples' surface morphology and cleavage were imaged by means of SEM, with the extremes, pDCMS grounded sample and MA-pDCMS  $3\times200$  W sample, selected as examples (Fig. 3). Clear differences can be observed between the two films. The pDCMS sample has a granular morphology of the fracture cross-section, which continues to the surface of the deposited film (Fig. 3A, B). The MA-pDCMS sample, exhibits faint columnar-like structuring, with a smooth surface without any distinguishable features (Fig. 3C, D).

Next, the films were characterised by means of Raman spectroscopy, stress measurements and nanoindentation (Fig. 4). The shape of the Raman spectra obtained from each sample closely resembles one another, especially between the MA-pDCMS samples. This is reflected by the results from nanoindentation, where the mechanical properties do not vary greatly. The elastic modulus remains relatively stable for all samples, independent of the applied fabrication method. In terms of hardness, the only substantial change is observed between the grounded and biased sample, from approx.  $24 \pm 1$  to  $30 \pm 1$  GPa. The addition of microwave plasma had no significant effect on the hardness, with respect to the non-MW biased sample. However, a clear increase in compressive film stress when applying a substrate bias during the growth was observed. The film stress continues to increase with the addition of microwave plasma until it eventually plateaus with increasing microwave power.

**Table 3**Fitted XRR results of pDCMS and MA-DCMS DLC films.

series	thickness profilometer (nm)	thickness XRR (nm)	density (g/cm³)
pDCMS, grounded	91	91	2.55
pDCMS, - 100 V bias	81	82	2.65
MA-pDCMS, 3×45 W	74	76	2.75
MA-pDCMS, 3×100 W	71	76	2.86
MA-pDCMS, $3\times200~W$	72	74	2.88

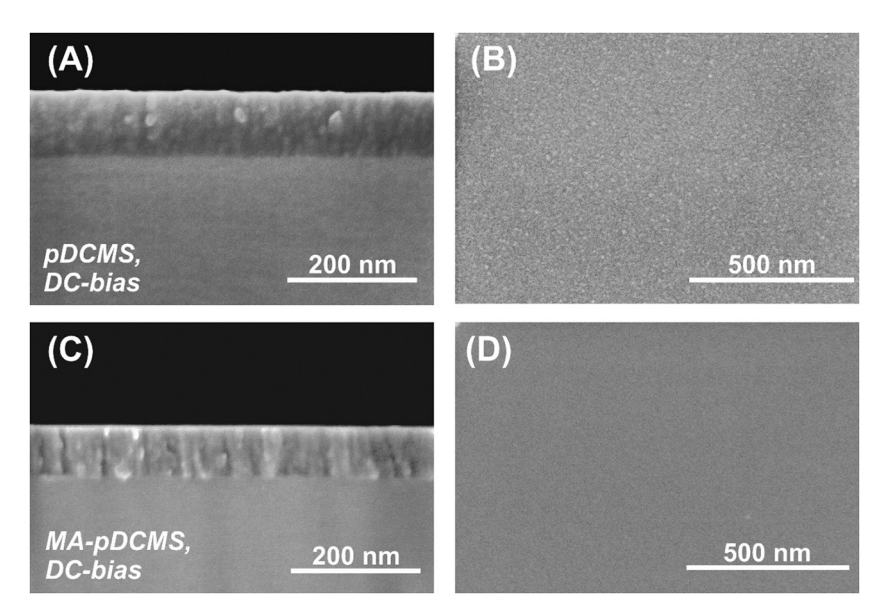
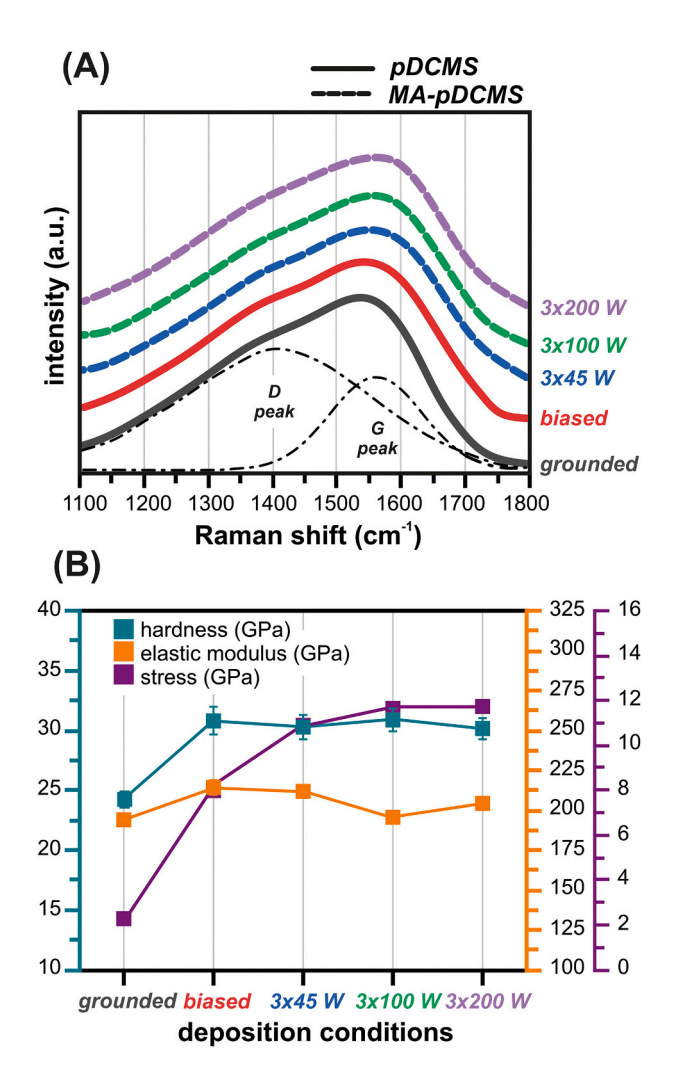


Fig. 3. SEM imaging of fracture surface and surface morphology of DLC films: (A, B) pDCMS with grounded DC substrate bias, (C, D) MA-pDCMS using 3×200 W MW power, with a DC substrate bias of -100 V.



**Fig. 4.** Results from (A) Raman spectroscopy, with marked D and G peak double Gaussian fitting of grounded pDCMS sample, (B) nanoindentation and film stress measurements of two pDCMS samples, grounded and -100~V substrate bias, and of three MA-pDCMS samples with -100~V substrate bias,  $3\times45~W$ ,  $3\times100~W$  and  $3\times200~W$ .

## 3.2. HiPIMS-based DLC films

## 3.2.1. HiPIMS plasma environment

The HiPSTER units are operated in a peak-current limiting mode, with a pulse length of 30  $\mu$ s at a repetition frequency of 600 Hz, translating to a duty cycle of 1.8 %. Feedback parameters for the 30 A limited setup are: voltage – 925 V, current 125 mA, average power 90 W and pulse charge  $\mu$ C.

The temporal evolution of voltage and current, carbon and argon emission intensities occurring during the HiPIMS are shown in Fig. 5. In this mode, the supply voltage rises to its maximum value of approx. – 925 V within 150 ns and gradually reduces to – 900 V towards the end of the 30  $\mu s$  pulse. It is further reduced to – 150 V within 10 ns, after which it is variated to ensure rapid decrease in pulse current. The discharge current increases exponentially from 0 A to 30 A during the 30  $\mu s$  pulse.

Langmuir probe measurements at the position of the substrate allowed to determine the properties of the HiPIMS plasma and the effect of microwave plasma during sputtering. The considered parameters were: plasma potential  $(V_p)$ , electron temperature  $(kT_e)$ , ion density  $(N_i)$  and electron density  $(N_e)$ . Firstly, the microwave plasma was analysed on its own to serve as a reference point for the MA-HiPIMS conditions. The power on each source was set at 50 W. As the microwave plasma was constant, measurements were conducted in time-averaged mode. The average plasma properties obtained from a single source and their joint effect are shown in Table 4.

The Langmuir probe results from HiPIMS and MA-HiPIMS are shown in Fig. 6. For the HiPIMS measurements, the probe was not able to obtain results for the first 5 µs, due to the large displacement currents induced by the HiPIMS voltage rise. The maximum plasma potential and electron temperature values are registered at the end of the pulse, with the maximum values for ion and electron density slightly after that. During the afterglow, the charged particles are released from the magnetron trap, enabling them to travel towards the substrate region. Following the afterglow, all values drop, which corresponds to the fact that the plasma is no longer ignited. Under MA-HiPIMS conditions, the first 20 µs show the properties of the microwave plasma (listed in Table 4). When the HiPIMS pulse starts at 20 μs, the Langmuir probe continues to operate normally, as the plasma generated by the microwave source shields the probe from the rapidly varying electric field generated by the target potential surge and no significant displacement currents are generated in the probe. Once the magnetron plasma ignites, the measured plasma properties decrease to values similar to those obtained during non-MW HiPIMS analysis. The plasma potential, electron temperature and ion density reach their minimum value just before the end of the pulse, whereas the electron density drops just after the end of the pulse. After the HiPIMS pulse has ended, the  $V_p$  and  $kT_e$  gradually rise until reaching the steady-state values of the microwave plasma. The same, however, cannot be said for the behaviour of the ion and electron densities. After the end of the pulse, the  $N_i$  and  $N_e$  values considerably exceed the original measured values, with their maximum measured 70  $\mu$ s after the end of the pulse. After reaching the maximum values, they gradually decrease until reaching the values of the originally-measured microwave plasma.

The temperature near the substrate was measured under pure HiPIMS and MA-HiPIMS to evaluate the possibility of material graphitisation, which occurs at temperatures exceeding 300  $^{\circ}\text{C}$  [9–11]. During sputtering, the temperature reaches a maximum temperature around 35  $^{\circ}\text{C}$ , whereas when turning on the microwave plasma, the temperature rises quickly and stabilises at approx. 130  $^{\circ}\text{C}$  (see supplementary information, Fig. S2).

#### 3.2.2. DLC film characterisation

The DC-bias HiPIMS and MA-HiPIMS, as well as pulsed-bias MA-HiPIMS fabricated DLC films were cleaved and analysed via SEM to determine their thickness, as well as surface morphology and fracture surface. Representative SEM images of samples produced at a substrate bias of – 250 V are shown in Fig. 7. The thickness of all HiPIMS-based films was homogeneous and in the range of 500 nm. The interface with the substrate can be clearly distinguished, with the films being free of cracks, pores, and signs of delamination, indicating that good quality films are attained. For the HiPIMS sample, faint columnar features can be seen on the fracture surface image, and the tops of those columns can be seen on the surface of the film. The MA-HiPIMS film appears to be much rougher, where both the cleavage and surface possess a randomly-orientated grainy morphology. In contrast, the MA-HiPIMS pulsed-bias sample's fracture surface has a clear columnar structure, while its

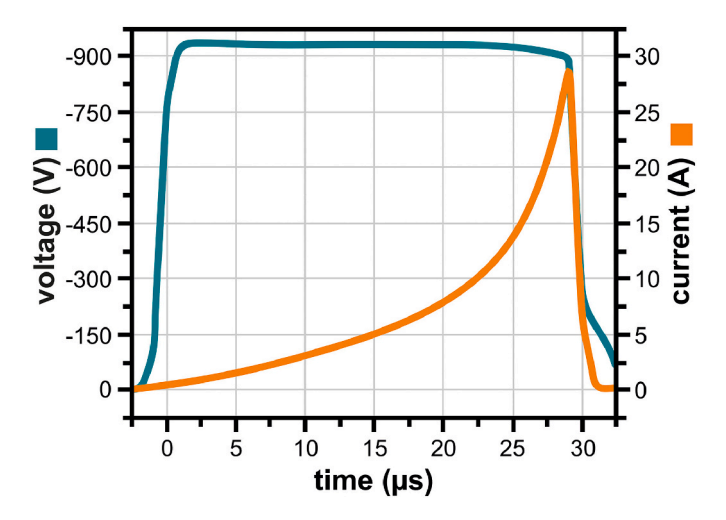
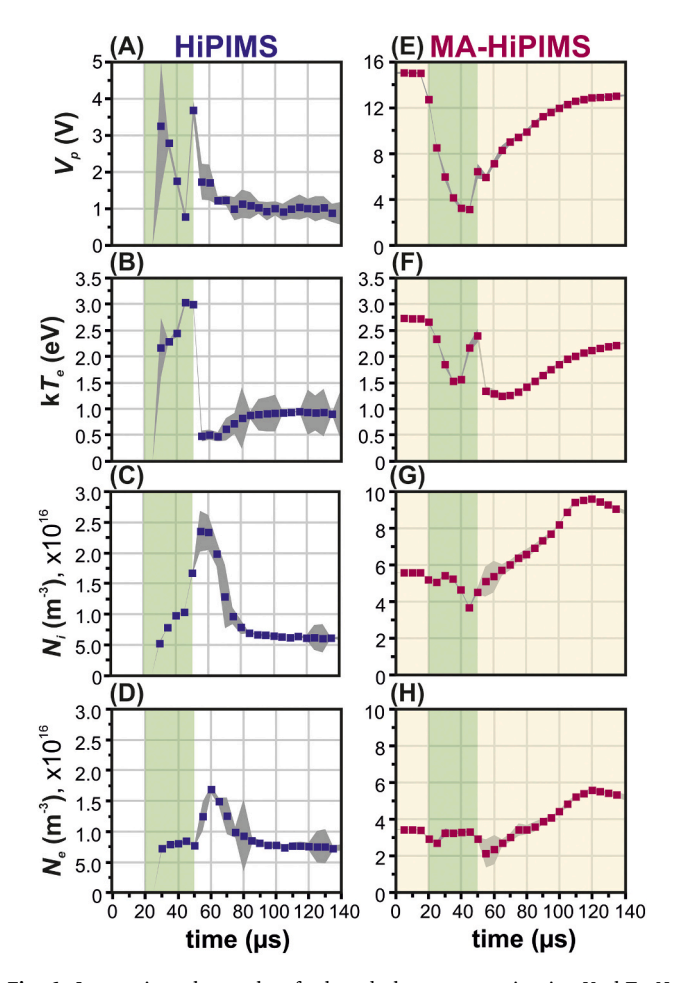


Fig. 5. Temporal evolution of HiPIMS pulse shape during 30  $\mu s.$ 

**Table 4**Ar microwave plasma properties generated by one source (averaged) and three sources.

No. of sources	$V_p$ (V)	$kT_e$ (eV)	$N_i  (\mathrm{m}^{-3})$	$N_e  (\mathrm{m}^{-3})$
1	$12.14\pm0.07$	$2.47\pm0.02$	$1.68 \times 10^{16} \pm$	9.57 × 10 <sup>15</sup> ±
3	$14.83 \pm 0.11$	$2.78 \pm 0.01$	$4.54 \times 10^{13}$ $5.32 \times 10^{16} \pm$ $2.96 \times 10^{14}$	$\begin{aligned} &1.28\times 10^{14}\\ &3.10\times 10^{16}\pm\\ &5.41\times 10^{14} \end{aligned}$



**Fig. 6.** Langmuir probe results of selected plasma properties, i.e.  $V_p$ ,  $kT_e$ ,  $N_b$  and  $N_e$ , at the location where the substrate would be, under: (A–D) HiPIMS and (E–H) MA-HiPIMS DLC sputtering conditions, grey areas mark measurement uncertainties, green areas mark pulse duration (30  $\mu$ s), yellow areas mark the period when only the microwave plasma is on, scales adapted to the data range.

surface has fewer features than the two previous samples, with only small grains being detected.

Next, Raman spectroscopy and nanoindentation were performed (Fig. 8), as well as XRR. Starting with the three HiPIMS series, a change in spectrum shape is observed with the change in bias voltage for all series, as well as small differences between each series (Fig. 8A, C, E). In all cases, peak broadening occurs with the increase in applied bias voltage. Additionally, films deposited at 0.4 Pa exhibit wider peaks than those deposited at 0.6 Pa. The hardness increased with increasing bias, with changes in Young's modulus resembling that of hardness. The maximum hardness value for each series is in the range of 25 GPa, whereas the minimum values differ between series deposited at different pressures, for 0.6 Pa approx. 5 GPa and 0.4 Pa, 10 GPa. Similar hardness trends as a function of substrate bias and working pressure have been reported in [33,46]. The density values obtained from XRR measurements correspond with the trend from nanoindentation, meaning that with an increasingly negative substrate bias, the density of the films increases, from approx. 2.6 g/cm<sup>3</sup> for the softest films up to approx. 2.9 g/cm<sup>3</sup> for the hardest ones. The obtained film densities are on the higher end of what has been reported for HiPIMS films [25,47,48], going into the density range of DLC films produced via pulsed laser deposition (PLD) [49] and filtered ion-beam deposition [50].

The results from the MA-HiPIMS series were set against the 0.4 Pa, 60 sccm Ar, HiPIMS series (Fig. 8E), as the only difference in deposition parameters is the presence of  $3\times50$  W microwave plasma in the former. When comparing the Raman spectra it can be seen that they greatly

resemble one another. Therefore, it was expected that the films'  $sp^2$  and  $sp^3$  hybridisation ratio would be similar, resulting in similar mechanical properties. However, when comparing the hardness and elastic modulus of these films, there are significant differences. On the example of the films produced at -250 V, the HiPIMS film had a hardness and elastic modulus of approx.  $25\pm1$  GPa and  $305\pm16$  GPa, respectively, whereas for the MA-HiPIMS film the obtained values were approx.  $8\pm1$  GPa and  $93\pm7$  GPa. Additionally, although MA-HiPIMS Raman spectra exhibit the same broadening effect with increasing bias voltage, a significant increase in mechanical properties only occurred at -300 V, rather a gradual increase like for the HiPIMS films. The density of the DC-bias MA-HiPIMS samples was approx. 2.3 g/cm³.

The Raman spectrum of the - 250 V pulsed-bias MA-HiPIMS sample closely resembled the DC-biased HiPIMS and MA-HiPIMS samples. The obtained hardness and elastic modulus were measured to be approx. 23  $\pm$  2 GPa and 234  $\pm$  15 GPa, respectively. Substituting DC-bias for pulsed-biasing allowed reaching a higher density of approx. 2.6 g/cm $^3$ .

#### 4. Discussion

#### 4.1. Plasma conditions vs DLC film properties

The selected pDCMS parameters for *system 1*, with a pulse-off setting of  $0.4~\mu s$ , repetition rate of 100~kHz and constant sputtering power of 300~kHz and constant sputtering power of 300~kHz and constant sputtering power of 300~kHz and versage pulse power of approx. 312.5~kHz and pulse energy of 0.003~jL With the distance between the target and the substrate set at 75~mm, and an applied pressure of 0.5~Pa, the mean free path is approx. 13~mm (assuming room temperature). This

means that the sputtered and argon species will experience on average 6 collisions on their way to the substrate. In the case of the applied HiPIMS parameters used in  $system\ 2$ , with a duty cycle of 1.8 %, the instantaneous power reaches 20 kW at the end of the pulse, with the pulse energy measured at 0.15 J, or an average pulse power of 5 kW for an average power of 90 W. The distance set between the target and the substrate was 120 mm. For pressures of 0.6 Pa and 0.4 Pa, the mean free paths were calculated to be approx. 10 and 16 mm, meaning an average collision rate of 12 and 8, respectively.

Within a single HiPIMS pulse, considerably higher plasma densities are assumed to be reached at the magnetron than during a pDCMS pulse, with average pulse power being 16-times greater for HiPIMS. This promotes the generation of ionised species. However, compared to *system 1* (with 6 collisions on average), there is a higher chance of the generated species to collide. These collisions will decrease the portion of ionised species impinging the substrate/growing film surface with an energy below the optimal value of 100 eV [4,16] for sp<sup>2</sup> to sp<sup>3</sup> transformation through both direct (carbon-induced) and indirect (argon-induced) subplantation (Fig. 1). This is supported by the comparison between nanoindentation results obtained for DLC films produced via HiPIMS (Fig. 8B, D, F) at different pressures (0.4 Pa and 0.6 Pa). At 0.4 Pa (avg. collision rate 8), a film hardness of approx. 20 GPa is attained using a substrate bias of – 50 V, whereas to reach similar hardness values at 0.6 Pa (avg. collision rate 12), a substrate bias of – 150 V is required.

Time-resolved Langmuir probe measurements under HiPIMS conditions enabled tracking the plasma properties of the magnetron during sputtering, as well as in the presence of microwave plasma. As was mentioned in the Results section, the maximum plasma potential and

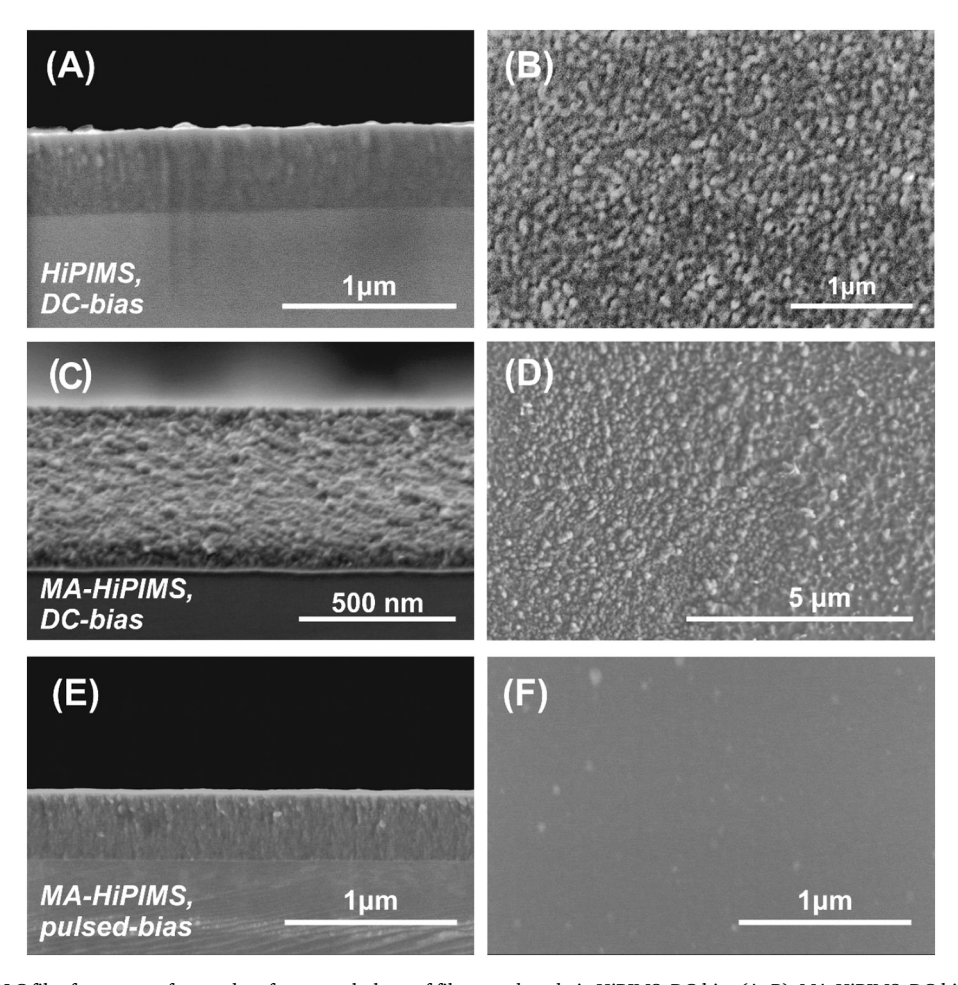


Fig. 7. SEM imaging of DLC film fracture surface and surface morphology of films produced via HiPIMS, DC-bias (A, B), MA-HiPIMS, DC-bias (C, D) and MA-HiPIMS, pulsed-bias (E, F), applied substrate bias – 250 V.

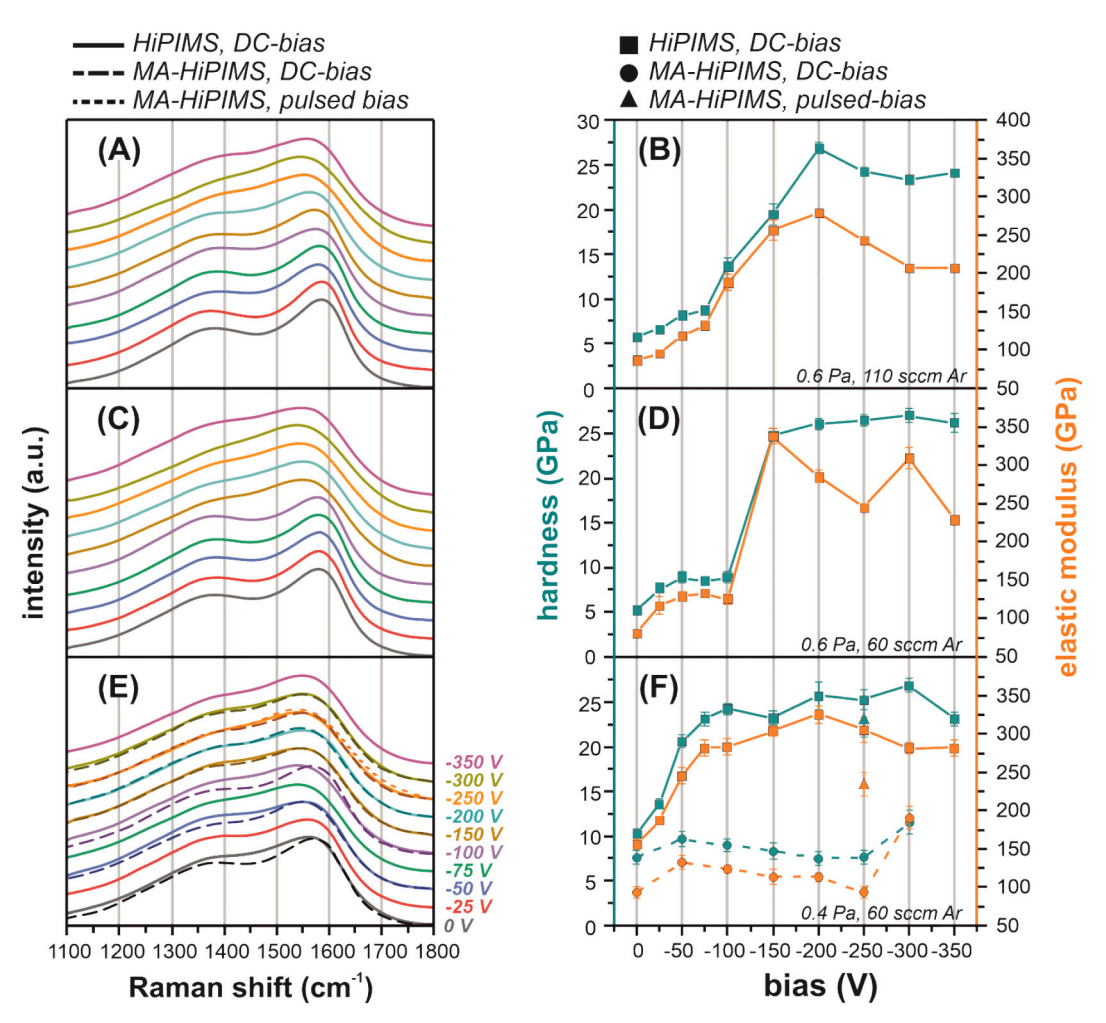


Fig. 8. Raman spectra and nanoindentation results of HiPIMS-based DLC films: (A, B) HiPIMS, 0.6 Pa and 110 sccm Ar flow, (C, D) HiPIMS, 0.6 Pa and 60 sccm Ar flow, and (E, F) HiPIMS, 0.4 Pa and 60 sccm Ar flow, MA-HiPIMS and pulsed-bias MA-HiPIMS; Raman spectra: HiPIMS (full line), MA-HiPIMS (dashed line), pulsed-bias MA-HiPIMS (dotted line); Nanoindentation: HiPIMS (square), MA-HiPIMS (circle), pulsed-bias MA-HiPIMS (triangle).

electron temperature in the substrate region are reached towards the end of the HiPIMS pulse, with the maximum values for ion and electron density reached slightly later, after the species have been released from the magnetron trap (Fig. 6A-D). Igniting the pulsed magnetron sources in the presence of continuous microwave plasma caused significant perturbations to its otherwise stable properties. During the HiPIMS pulse-on time, the plasma properties change from the values observed for the continuous microwave plasma to values typical for the HiPIMS mode. This behaviour can be attributed to the electric field generated by the high voltage supplied to the target, which is not yet shielded by the just-developing high density plasma in the vicinity of the target. Similar effects have been observed in pulsed RF discharges [51], with the interpretation being further supported by the registered strong perturbation of the Langmuir probe operation during HiPIMS pulse onset in the absence of the volume MW plasma. The generated negative electric field draws the argon ions of the MW plasma towards the magnetrons causing the observed decrease in all analysed plasma properties in the vicinity of the probe (substrate height). The highest ion and electron densities at the substrate area are observed after the end of the HiPIMS pulse, in the presence of the MW plasma. Here, the microwave plasma enhances the transfer of charged particles from the dense plasma generated at the target towards the substrate.

Neither the use of microwave plasma nor the change in substrate biasing affected the deposition rates of pDCMS- and HiPIMS-processes, which were approx. 8.6 nm/min and 1.6 nm/min, respectively. The former is much greater than the latter, due to its much higher duty

cycle. The deposited DLC films from both pDCMS and HiPIMS processes without microwave plasma were characterised by a mostly granular-like fracture surface, which was additionally reflected by a granular surface morphology (Figs. 3A, B and 7A, B, respectively). With the addition of microwave plasma for MA-pDCMS processes, the DLC film's cleaved surface became columnar-like, without any characteristic features on its surface (Fig. 3C, D). Furthermore, the film's density increased from  $2.55 \text{ g/cm}^3$  for the grounded pDCMS film to  $2.88 \text{ g/cm}^3$  for the -100 V, 3×200 W MA-pDCMS sample (Table 3). DLC film densification can be explained by following the evolution in substrate current with changing processing conditions, depicted in Fig. 9. The current rises from 0 mA for the former to a maximum of 175 mA for the latter, which is linked with the generation of high plasma densities (and high current densities) by the microwave plasma sources (for estimations on plasma properties generated within system 1, see supplementary information Table S1). In turn, densification through indirect subplantation (Fig. 1) most probably occurred, as an increase in internal film stress was also registered (Fig. 4B). In the case of DLC films produced via MA-HiPIMS with DC substrate biasing, a different effect was observed. The films exhibited increased granularity of both the fracture cross-section and surface morphology in comparison to the HiPIMS-deposited films, with the DLC film density and mechanical properties also decreasing to approx. 2.3 g/cm<sup>3</sup> and  $H=8\pm1$  GPa,  $E=93\pm7$  GPa (for -250 V substrate bias), respectively. Comparing MA-pDCMS and MA-HiPIMS substrate currents for the same substrate bias (-100 V) and similar microwave powers (3×45 W vs 3×50 W), similar values were measured. The main

difference lies in the positioning of the microwave sources, where for MA-pDCMS the sources placed at the sputtering target, and for MA-HiPIMS, are at the height of the substrate. It is at those positions that the argon plasma density will be the greatest. Therefore, the MA-HiPIMS-produced films will more likely be subjected to high-energy Ar ion bombardment [52]. Rather than generating sp<sup>3</sup> bonds due to indirect subplantation (Fig. 1), the authors believe that the bombardment could have caused local temperature spikes that were not registered by the temperature probe and resulting in film graphitisation. Based on the previously-performed Langmuir probe measurements (Fig. 6), a substrate bias pulsing strategy was developed for the MA-HiPIMS process so that the bias was only applied once the generated carbon species were released from the magnetron trap, decreasing the effect of Ar-ion bombardment. The measured substrate currents resembled those registered for HiPIMS processes without microwave plasma, which corresponds to the similar plasma properties obtained from Langmuir probe measurements. The films fracture cross-section and surface morphology resemble that of the MA-pDCMS sample, exhibiting columnar structuring and a surface with few characteristic features (Fig. 3E, F). The pulsed-bias DLC film had a higher density of 2.6 g/cm<sup>3</sup> than its DC-biased counterpart. The measured mechanical properties were also higher, i.e.  $H=23\pm2$  GPa and  $E=234\pm15$  GPa. These results highlight the importance of microwave plasma source positioning in respect to the substrate, as it can have a detrimental effect on the quality of the produced films.

## 4.2. DLC film structuring

Raman spectroscopy exhibits sensitivity to changes in the carbon structure, e.g. crystallinity, carbon bonds and clustering. There are two main peaks in the Raman spectra of amorphous carbon, i.e. the D band appearing at approx.  $1355~{\rm cm}^{-1}$  and the G band at approx.  $1581~{\rm cm}^{-1}$ . The D band appears due to the A1g breathing mode and requires a defect for its activation. The G band originates from the E2g stretching mode and occurs at all available  ${\rm sp}^2$  sites, rings, or chains. Explanations behind the interpretation of the obtained spectra are provided by Ferrari et al. [53–55], where the transition mechanism and Raman spectroscopy response from graphite to tetrahedral amorphous carbon (ta-C) DLC is proposed, by correlating the evolution of D and G peak intensity ratios ( $I_D/I_G$ ) with the migration of the G peak shift. This transition is referred to as the *amorphization trajectory*. Three transition stages are distinguished: (1) from graphite to nanocrystalline (nc) graphite, where only

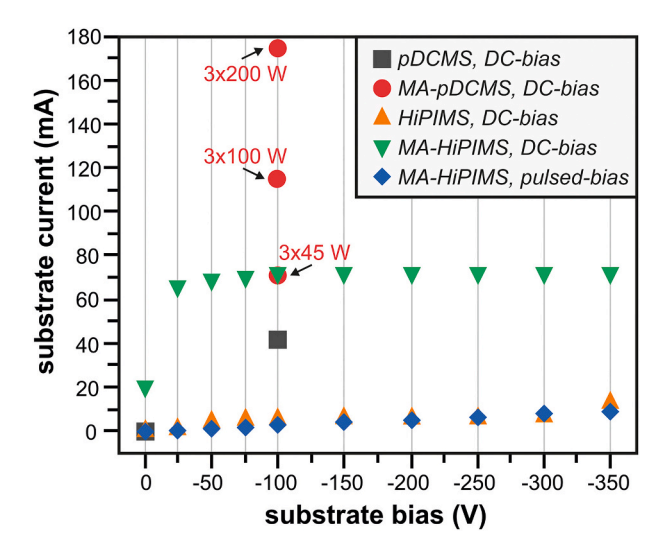


**Fig. 9.** Substrate currents, as a function of substrate bias, registered during pDCMS, MA-pDCMS (with marked applied microwave plasma power), HiPIMS with DC substrate biasing and MA-HiPIMS with pulsed substrate biasing (see legend for details).

sp<sup>2</sup>-type hybridisations are present, (2) from nc-graphite to amorphous carbon, and (3) from a-C to ta-C. The Raman spectra obtained from pDCMS-based methods did not show any distinct trends, with the spectra closely resembling one another (Fig. 4). The spectra obtained from HiPIMS-based DLC samples (Fig. 8) showed a broadening effect with increasing substrate bias. The broadening effect results from a higher level of disorder within the amorphous structure [56] of the fabricated DLC films. When considering the amorphization trajectory from graphite to tetrahedral amorphous carbon, there are many possible intermediate configurations of carbon atoms (rings, partial rings, chains) [57] that may occur and cannot be determined with certainty. However, each configuration will have its own vibrational frequency, which will be detected by Raman spectroscopy. With the increase in various carbon configurations randomly distributed throughout the amorphous structure of the DLC film, more signals will be registered, and the corresponding peaks will overlap over one another, causing overall peak widening. When comparing the measured hardness with the previously analysed Raman spectra, it can be noticed that peak broadening coincides with hardness increase. This may suggest that a higher level of disorder of carbon configurations (also film densification and the presence of residual stress) within the films' amorphous structures induces a certain strengthening effect, resulting in higher hardness. The Raman spectra of all produced DLC films were deconvoluted to determine if any further trends could be observed by tracking the evolution of  $I_D/I_G$  ratio as a function of G peak position (Fig. 10A, B), and G peak FWHM as a function of measured film hardness (Fig. 10C).

Following the obtained  $I_D/I_G$  ratios and G peak positions, it was determined that the produced DLC films lie within the 2nd amorphization stage (Fig. 10A), however, no trends could be distinguished, with most of the films falling within the same value range (Fig. 10B). The provided example hardness values further highlight the lack of trends, as based on the amorphization trajectory, films with similar  $I_D/I_G$  ratios and G peak positions should have similar sp<sup>2</sup>/sp<sup>3</sup> contents and, in turn, similar mechanical properties would be expected. Indeed, deviations from the ideal three-stage amorphization trajectory model of nonhydrogenated films have been previously reported [58]. This is especially true when comparing the previously shown HiPIMS and MA-HiPIMS (0.4 Pa, 60 sccm Ar) results, where the Raman spectra and G peak FWHM closely resemble one another, however, the HiPIMS film had a hardness of approx. 25  $\pm$  1 GPa and the MA-HiPIMS had a hardness of approx.  $8 \pm 1$  GPa (for a substrate bias of -250 V). When tracking G peak FWHM changes as a function of DLC film hardness (Fig. 10C), for almost all produced DLC films the FWHM increases with increasing hardness. The exception is the MA-HiPIMS DC-bias series, where similar FWHM values were obtained as for the HiPIMS series, however, the hardness values are significantly lower. This in in agreement with the Raman spectra broadening trends observed in Fig. 8. For a FWHM value of around 125, the MA-HiPIMS sample has a hardness of  $8\pm1$  GPa, whereas the HiPIMS sample possesses a hardness of 26  $\pm$  2 GPa. The main characteristic differentiating the MA-HiPIMS DC-bias series from all other deposited films is its highly granular structure, as observed via SEM (Figs. 3 and 7) and has been determined to be the contributing factor. Based on these results, using the G peak FWHM provides a more solid basis for DLC results interpretation, however, it should be highlighted that Raman spectroscopy, although a useful technique, is unable to "see" all the factors contributing to DLC material structuring.

#### 5. Conclusions

In this work, DLC films were produced by means of pDCMS, MA-pDCMS, HiPIMS, MA-HiPIMS with DC substrate biasing and MA-HiPIMS with pulsed substrate biasing. The aim of comparing these techniques was to provide an improved understanding on the correlation between the generated deposition environment, especially plasma conditions, and the properties of the fabricated DLC films. For both cases, it was demonstrated that standard sputtering cathodes can be

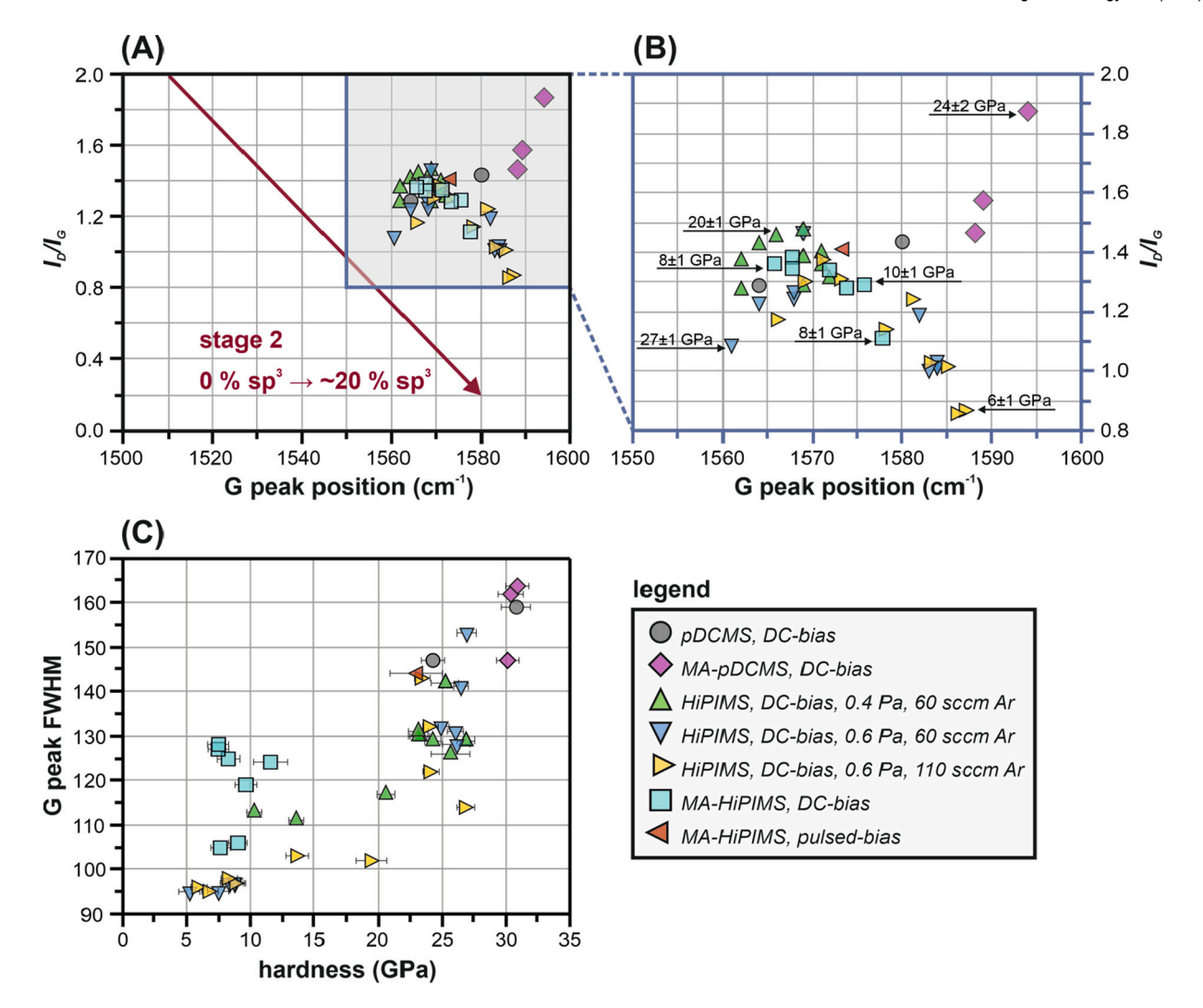


**Fig. 10.** Raman spectra interpretation of all fabricated DLC films (see legend for deposition method symbols), where: (A)  $I_D/I_G$  ratio as a function of G peak position within the full amorphization trajectory range from graphite to ta-C [53,54] with the 2nd stage range (nc-graphite to a-C, 0–20 % sp<sup>3</sup>) marked with a red arrow, (B) experimental result range of  $I_D/I_G$  ratio vs G peak position with hardness values included for selected samples, and (C) G peak FWHM as a function of measured DLC film hardness.

arranged close to microwave plasma sources. The inclusion of high-density microwave plasmas can be used to increase the ion current present at the substrate during film growth, enabling a modification of the physical properties of the fabricated layer. An intriguing point that can be noted by comparing the results obtained from all studied deposition methods, is that despite using various microwave source configurations and sputtering conditions, the upper hardness limit for DLC films fluctuated around 30 GPa. This shows the limitation of sputtering and the challenge of increasing the ionisation of carbon. The initial idea of post-ionisation via microwave plasma did not have a significant effect in reaching higher hardness values, however, it did contribute to attaining smoother surfaces in both pDCMS- and HiPIMS-based methods, which could prove to be beneficial for DLC films working under wear conditions.

### CRediT authorship contribution statement

Caroline Hain: conceptualisation, depositions, investigations and analysis, preparing original draft, graphics; David Brown: depositions, investigations and analysis, draft revision and editing; Alexander Welsh: investigations and analysis, draft revision and editing; Krzysztof

Wieczerzak: investigations and analysis, draft revision and editing; Robert Weiss: supervision, hardware integration, draft revision and editing; Johann Michler: supervision, resources, draft revision and editing; Aïcha Hessler-Wyser: supervision, draft revision and editing; Thomas Nelis: conceptualisation, supervision, resources, draft revision and editing.

## Declaration of competing interest

The authors declare that they have no known competing financial interests or personal relationships that could have appeared to influence the work reported in this paper.

## Acknowledgements

The authors would like to acknowledge and thank Dr. Nadim Scherrer of HKB BFH for providing access and assistance with Raman spectroscopy, as well as Petai Pip of Empa Thun for assistance with XRR measurements and fitting procedures. The authors gratefully acknowledge financial support through EUROSTARS (Plasma S3Tream E! 12507) and the National Science Foundation (SBIR Award #1853254). K.W.

acknowledges the EMPAPOSTDOCS-II programme that has received funding from the European Union's Horizon 2020 research programme under the Marie Skłodowska-Curie grant agreement number 754364.

## Appendix A. Supplementary information

Supplementary data to this article can be found online at https://doi.org/10.1016/j.surfcoat.2021.127928.

#### References

- A.C. Ferrari, Diamond-like carbon for magnetic storage disks, Surf. Coat. Technol. 180–181 (2004) 190–206, https://doi.org/10.1016/J.SURFCOAT.2003.10.146.
- [2] A. Grill, Diamond-like carbon: state of the art, Diam. Relat. Mater. 8 (1999) 428–434, https://doi.org/10.1016/S0925-9635(98)00262-3.
- [3] T.F. Zhang, Q.Y. Deng, B. Liu, B.J. Wu, F.J. Jing, Y.X. Leng, N. Huang, Wear and corrosion properties of diamond like carbon (DLC) coating on stainless steel, CoCrMo and Ti6Al4V substrates, Surf. Coat. Technol. 273 (2015) 12–19, https:// doi.org/10.1016/J.SURFCOAT.2015.03.031.
- [4] K. Bewilogua, D. Hofmann, History of diamond-like carbon films from first experiments to worldwide applications, Surf. Coat. Technol. 242 (2014) 214–225, https://doi.org/10.1016/J.SURFCOAT.2014.01.031.
- [5] J. Robertson, Comparison of diamond-like carbon to diamond for applications, Phys. Status Solidi 205 (2008) 2233–2244, https://doi.org/10.1002/ pssa.200879720.
- [6] C. Jaoul, O. Jarry, P. Tristant, T. Merle-Méjean, M. Colas, C. Dublanche-Tixier, J.-M. Jacquet, Raman analysis of DLC coated engine components with complex shape: understanding wear mechanisms, Thin Solid Films 518 (2009) 1475–1479, https://doi.org/10.1016/J.TSF.2009.09.110.
- [7] C. Saringer, C. Oberroither, K. Zorn, R. Franz, C. Mitterer, Influence of discharge power and bias potential on microstructure and hardness of sputtered amorphous carbon coatings, J. Vac. Sci. Technol. A 36 (2018), 021501, https://doi.org/ 10.1116/1.5001141.
- [8] X. Peng, Z. Barber, T. Clyne, Surface roughness of diamond-like carbon films prepared using various techniques, Surf. Coat. Technol. 138 (2001) 23–32, https://doi.org/10.1016/S0257-8972(00)01139-7.
- [9] R. Kalish, Y. Lifshitz, K. Nugent, S. Prawer, Thermal stability and relaxation in diamond-like-carbon. A raman study of films with different sp3 fractions (ta-C to a-C), Appl. Phys. Lett. 74 (1999) 2936–2938, https://doi.org/10.1063/1.123971.
- [10] D.R. Tallant, J.E. Parmeter, M.P. Siegal, R.L. Simpson, The thermal stability of diamond-like carbon, Diam. Relat. Mater. 4 (1995) 191–199, https://doi.org/ 10.1016/0925-9635(94)00243-6.
- [11] M. He, C. Yeo, Evaluation of thermal degradation of DLC film using a novel raman spectroscopy technique, Coatings 8 (2018) 143, https://doi.org/10.3390/ coatings8040143
- [12] Z. Chen, X. He, C. Xiao, S. Kim, Effect of humidity on friction and wear—acritical review, Lubricants 6 (2018) 74, https://doi.org/10.3390/lubricants6030074.
- [13] H. Li, T. Xu, C. Wang, J. Chen, H. Zhou, H. Liu, Effect of relative humidity on the tribological properties of hydrogenated diamond-like carbon films in a nitrogen environment, J. Phys. D. Appl. Phys. 38 (2005) 62–69, https://doi.org/10.1088/ 0023.3727/89.1.011
- [14] C. Donnet, A. Erdemir, Tribology of Diamond-Like Carbon Films, Springer US, Boston, MA, 2008, https://doi.org/10.1007/978-0-387-49891-1.
- [15] S.R. Kasi, J.W. Rabalais, W. Eckstein, Y. Llfshitz, Subplantation model for film growth from hyperthermal species, Phys. Rev. B 41 (1990), 10 468-10 480.
- [16] J. Robertson, The deposition mechanism of diamond-like a-C and a-C: H, Diam. Relat. Mater. 3 (1994) 361–368, https://doi.org/10.1016/0925-9635(94)90186-4.
- [17] J. Annaloro, V. Morel, A. Bultel, P. Omaly, Global rate coefficients for ionization and recombination of carbon, nitrogen, oxygen, and argon, Phys. Plasmas. 19 (2012), 073515, https://doi.org/10.1063/1.4737147.
- [18] J.T. Gudmundsson, N. Brenning, D. Lundin, U. Helmersson, High power impulse magnetron sputtering discharge, J. Vac. Sci. Technol. A 30 (2012), 030801, https://doi.org/10.1116/1.3691832.
- [19] C. Christou, Z.H. Barber, Ionization of sputtered material in a planar magnetron discharge, J. Vac. Sci. Technol. A 18 (2000) 2897–2907, https://doi.org/10.1116/ 1.1312370
- [20] A. Anders, A review comparing cathodic arcs and high power impulse magnetron sputtering (HiPIMS), Surf. Coat. Technol. 257 (2014) 308–325, https://doi.org/ 10.1016/j.surfcoat.2014.08.043.
- [21] H. Takikawa, K. Izumi, R. Miyano, T. Sakakibara, DLC thin film preparation by cathodic arc deposition with a super droplet-free system, Surf. Coat. Technol. 163–164 (2003) 368–373, https://doi.org/10.1016/S0257-8972(02)00629-1.
- [22] J. Vetter, 60 years of DLC coatings: historical highlights and technical review of cathodic arc processes to synthesize various DLC types, and their evolution for industrial applications, Surf. Coat. Technol. 257 (2014) 213–240, https://doi.org/ 10.1016/J.SURFCOAT.2014.08.017.
- [23] J.W. Bradley, H. Bäcker, P.J. Kelly, R.D. Arnell, Space and time resolved langmuir probe measurements in a 100 kHz pulsed rectangular magnetron system, Surf. Coat. Technol. 142–144 (2001) 337–341, https://doi.org/10.1016/S0257-8972 (01)01084-2.
- [24] J.W. Bradley, H. Bäcker, P.J. Kelly, R.D. Arnell, Time-resolved langmuir probe measurements at the substrate position in a pulsed mid-frequency DC magnetron

- plasma, Surf. Coat. Technol. 135 (2001) 221–228, https://doi.org/10.1016/S0257-8972(00)00990-7.
- [25] K. Sarakinos, A. Braun, C. Zilkens, S. Mráz, J.M.M. Schneider, H. Zoubos, P. Patsalas, Exploring the potential of high power impulse magnetron sputtering for growth of diamond-like carbon films, Surf. Coat. Technol. 206 (2012) 2706–2710, https://doi.org/10.1016/J.SURFCOAT.2011.11.032.
- [26] K. Sarakinos, J. Alami, S. Konstantinidis, High power pulsed magnetron sputtering: a review on scientific and engineering state of the art, Surf. Coat. Technol. 204 (2010) 1661–1684, https://doi.org/10.1016/J.SURFCOAT.2009.11.013.
- [27] A.P. Ehiasarian, High-power impulse magnetron sputtering and its applications, Pure Appl. Chem. 82 (2010) 1247–1258, https://doi.org/10.1351/PAG-CON-09-10-43
- [28] J. Paulitsch, M. Schenkel, T. Zufraß, P.H. Mayrhofer, W.-D. Münz, Structure and properties of high power impulse magnetron sputtering and DC magnetron sputtering CrN and TiN films deposited in an industrial scale unit, Thin Solid Films 518 (2010) 5558–5564, https://doi.org/10.1016/J.TSF.2010.05.062.
- [29] M. Hiratsuka, A. Azuma, H. Nakamori, Y. Kogo, Extraordinary deposition rate of diamond-like carbon film using HIPIMS technology, Surf. Coat. Technol. 229 (2013) 46–49, https://doi.org/10.1016/J.SURFCOAT.2012.06.016.
- [30] T. Konishi, K. Yukimura, K. Takaki, Fabrication of diamond-like carbon films using short-pulse HiPIMS, Surf. Coat. Technol. 286 (2016) 239–245, https://doi.org/ 10.1016/J.SURFCOAT.2015.12.010.
- [31] J.A. Santiago, I. Fernández-Martínez, T. Kozák, J. Capek, A. Wennberg, J. M. Molina-Aldareguia, V. Bellido-González, R. González-Arrabal, M.A. Monclús, The influence of positive pulses on HiPIMS deposition of hard DLC coatings, Surf. Coat. Technol. 358 (2019) 43–49, https://doi.org/10.1016/J. SURFCOAT.2018.11.001.
- [32] F. Ferreira, A. Cavaleiro, J. Oliveira, Tribological performance of DLC coatings deposited by DOMS in mixed ar-ne discharges, Mater. Lett. 285 (2021), 129056, https://doi.org/10.1016/j.matlet.2020.129056.
- [33] J. Oliveira, F. Ferreira, R. Serra, T. Kubart, C. Vitelaru, A. Cavaleiro, Correlation between substrate ion fluxes and the properties of diamond-like carbon films deposited by deep oscillation magnetron sputtering in ar and ar + ne plasmas, Coatings 10 (2020) 914, https://doi.org/10.3390/COATINGS10100914.
- [34] T. Kubart, A. Aijaz, J. Andersson, F. Ferreira, J.C. Oliveira, A. Sobetkii, A.C. Parau, C. Vitelaru, High power impulse magnetron sputtering of diamond-like carbon coatings, J. Vac. Sci. Technol. A 38 (2020), 043408, https://doi.org/10.1116/6.0000070.
- [35] B.M. DeKoven, P.R. Ward, R.E. Weiss, D.J. Christie, R.A. Scholl, W.D. Sproul, F. Tomasel, A. Anders, Carbon thin film deposition using high power pulsed magnetron sputtering, in: Proceedings, Annu. Tech. Conf. - Soc. Vac. Coaters, 2003, pp. 158–165.
- [36] A. Aijaz, K. Sarakinos, D. Lundin, N. Brenning, U. Helmersson, A strategy for increased carbon ionization in magnetron sputtering discharges, Diam. Relat. Mater. 23 (2012) 1-4, https://doi.org/10.1016/J.DIAMOND.2011.12.043.
- [37] E. Kamijo, T. Nakamura, Y. Tani, AFM observations of DLC films prepared by the ECR sputtering method, Nucl. Instrum. Methods Phys. Res., Sect. B 121 (1997) 110–115, https://doi.org/10.1016/S0168-583X(96)00542-3.
- [38] J. Pang, W. Lu, Y. Xin, H. Wang, J. He, J. Xu, Plasma diagnosis for microwave ECR plasma enhanced sputtering deposition of DLC films, Plasma Sci. Technol. 14 (2012) 172–176, https://doi.org/10.1088/1009-0630/14/2/17.
- [39] L. Latrasse, M. Radoiu, T. Nelis, O. Antonin, Self-matching plasma sources using 2.45 GHz solid-state generators: microwave design and operating performance, J. Microw. Power Electromagn. Energy 51 (2017) 237–258, https://doi.org/ 10.1080/08327823.2017.1388338.
- [40] G.G. Stoney, The tension of metallic films deposited by electrolysis, Proc. R. Soc. London, Ser. A 82 (1909) 172–175, https://doi.org/10.1098/rspa.1909.0021.
- [41] T. Chudoba, P. Schwaller, R. Rabe, J.-M. Breguet, J. Michler, Comparison of nanoindentation results obtained with berkovich and cube-corner indenters, Philos. Mag. 86 (2006) 5265–5283, https://doi.org/10.1080/ 14786430600746424.
- [42] W.C. Oliver, G.M. Pharr, An improved technique for determining hardness and elastic modulus using load and displacement sensing indentation experiments, J. Mater. Res. 7 (1992) 1564–1583, https://doi.org/10.1557/JMR.1992.1564.
- [43] S. Cho, I. Chasiotis, T.A. Friedmann, J.P. Sullivan, Young's modulus, Poisson's ratio and failure properties of tetrahedral amorphous diamond-like carbon for MEMS devices, J. Micromech. Microeng. 15 (2005) 728–735, https://doi.org/10.1088/ 0960-1317/15/4/009.
- [44] S.-J. Cho, K.-R. Lee, K. Yong Eun, J. Hee Hahn, D.-H. Ko, Determination of elastic modulus and Poisson's ratio of diamond-like carbon films, Thin Solid Films 341 (1999) 207–210, https://doi.org/10.1016/S0040-6090(98)01512-0.
- [45] L. Liu, T. Wang, J. Huang, Z. He, Y. Yi, K. Du, Diamond-like carbon thin films with high density and low internal stress deposited by coupling DC/RF magnetron sputtering, Diam. Relat. Mater. 70 (2016) 151–158, https://doi.org/10.1016/j. diamond.2016.10.004.
- [46] J. Lin, W.D. Sproul, R. Wei, R. Chistyakov, Diamond like carbon films deposited by HiPIMS using oscillatory voltage pulses, Surf. Coat. Technol. 258 (2014) 1212–1222, https://doi.org/10.1016/J.SURFCOAT.2014.06.061.
- [47] S. Nakao, K. Yukimura, H. Ogiso, S. Nakano, T. Sonoda, Effects of ar gas pressure on microstructure of DLC films deposited by high-power pulsed magnetron sputtering, Vacuum 89 (2013) 261–266, https://doi.org/10.1016/J. VACUUM.2012.07.004.
- [48] F. Ferreira, A. Aijaz, T. Kubart, A. Cavaleiro, J. Oliveira, Hard and dense diamond like carbon coatings deposited by deep oscillations magnetron sputtering, Surf. Coat. Technol. 336 (2018) 92–98, https://doi.org/10.1016/J. SURFCOAT.2017.10.055.

- [49] P. Patsalas, S. Kaziannis, C. Kosmidis, D. Papadimitriou, G. Abadias, G. A. Evangelakis, Optimized pulsed laser deposition by wavelength and static electric field control: the case of tetrahedral amorphous carbon films, J. Appl. Phys. 101 (2007), 124903, https://doi.org/10.1063/1.2745445.
- [50] P.J. Fallon, V.S. Veerasamy, C.A. Davis, J. Robertson, G.A.J. Amaratunga, W. I. Milne, J. Koskinen, Properties of filtered-ion-beam-deposited diamondlike carbon as a function of ion energy, Phys. Rev. B 48 (1993) 4777–4782, https://doi.org/10.1103/PhysRevB.48.4777.
- [51] R. Valledor, P. Vega, J. Pisonero, T. Nelis, N. Bordel, Further insights into prepeak emission in pulsed radiofrequency glow discharge, Spectrochim. Acta B At. Spectrosc. 85 (2013) 45–54, https://doi.org/10.1016/j.sab.2013.04.002.
- [52] B. Akhavan, R. Ganesan, M. Stueber, S. Ulrich, D.R. McKenzie, M.M.M. Bilek, Carbon films deposited by mixed-mode high power impulse magnetron sputtering for high wear resistance: the role of argon incorporation, Thin Solid Films 688 (2019), 137353, https://doi.org/10.1016/j.tsf.2019.06.003.
- [53] A.C. Ferrari, J. Robertson, Interpretation of raman spectra of disordered and amorphous carbon, Phys. Rev. B 61 (2000) 14095–14107, https://doi.org/ 10.1103/PhysRevB.61.14095.

- [54] A.C. Ferrari, J. Robertson, Raman spectroscopy of amorphous, nanostructured, diamond-like carbon, and nanodiamond, Philos. Trans. R. Soc. London, Ser. A 362 (2004) 2477–2512, https://doi.org/10.1098/rsta.2004.1452.
- [55] A.C. Ferrari, Determination of bonding in diamond-like carbon by raman spectroscopy, Diam. Relat. Mater. 11 (2002) 1053–1061, https://doi.org/10.1016/ S0925-9635(01)00730-0.
- [56] J. Kabel, T.E.J. Edwards, C. Hain, T. Kochetkova, D. Parkison, J. Michler, P. Hosemann, A novel fiber-fretting test for tribological characterization of the fiber/matrix interface, Compos. Part B 206 (2021), 108535, https://doi.org/ 10.1016/j.compositesb.2020.108535.
- [57] D. Lin-Vien, W.G. Fateley, N.B. Colthup, J.G. Grasselli. The Handbook of Infrared and Raman Characteristic Frequencies of Organic Molecules, Academic Press, 1991. https://www.sciencedirect.com/book/9780124511606/the-handbook-ofinfrared-and-raman-characteristic-frequencies-of-organic-molecules.
- [58] L. Zhang, X. Wei, Y. Lin, F. Wang, A ternary phase diagram for amorphous carbon, Carbon N. Y. 94 (2015) 202–213, https://doi.org/10.1016/J. CARBON.2015.06.055.